Published online: June 30, 2019

Original Research

Modulation of NMDA-mediated intrinsic membrane properties of ascending commissural interneurons in neonatal rat spinal cord

Yi Cheng[1], Renkai Ge[2,3], Ke Chen[2] and Yue Dai[1,2,*]

[1] *Key Laboratory of Adolescent Health Assessment and Exercise Intervention of Ministry of Education, School of Physical Education and Health Care, East China Normal University, Shanghai, 200241, P. R. China*

[2] *Shanghai Key Laboratory of Multidimensional Information Processing, School of Information Science Technology, East China Normal University, Shanghai, 200241, P. R. China*

[3] *School of Physical Education and Health Care, East China Jiaotong University, Nanchang, 330013, P. R. China*

*Correspondence: ydai@tyxx.ecnu.edu.cn (Yue Dai)

DOI: 10.31083/j.jin.2019.02.129

In this paper, the modulation of ascending commissural interneurons by N-methyl-D-aspartate was investigated in neonatal rats by using retrograde labeling and whole-cell patch clamp. Data shows these interneurons can be divided into three types (single spike, phasic, and tonic) based on their firing patterns. A hyperpolarization-activated nonselective cation current and persistent inward current are expressed in these interneurons. The parameters studied (n = 48) include: resting membrane potential (-59.2 ± 0.8 mV), input resistance (964.4 ± 49.3 MΩ), voltage threshold (-39.5 ± 0.6 mV), rheobase (13.5 ± 0.7 pA), action potential height (55.6 ± 2.2 mV), action potential half-width (2.8 ± 0.1 ms), after-hyperpolarization magnitude (16.1 ± 1.2 mV) and half-decay (217.9 ± 10.7ms). 10 μM N-methyl-D-aspartate increases excitability of ascending commissural interneurons by depolarizing the membrane potential, hyperpolarizing voltage threshold, reducing rheobase, and shifting the frequency-current relationship to the left. N-methyl-D-aspartate enhances persistent inward currents but reduces hyperpolarization-activated nonselective cation currents. This research uncovers unique ionic and intrinsic properties of ascending commissural interneurons which can be modulated by major excitatory neurotransmitters such as N-methyl-D-aspartate to potentially facilitate left-right alternation during locomotion.

Keywords

Commissural interneurons; neuronal excitability; NMDA modulation; locomotion; spinal cord

1. Introduction

Locomotion is a fundamental motor behavior in vertebrates such as walking, crawling, swimming, and flying. These movements are characterized as rhythmic activities of flexor and extensor motoneurons and periodic alternation of left and right limbs. They are generated by the spinal neural networks known as central pattern generators (CPG) (Kiehn, 2005). Commissural interneurons (CINs) are one of specific component of the CPG which project axons to the contralateral side of the spinal cord and play a crucial role in coordinating the left-right alternation of limb movement during locomotion (Jankowska, 2008; Nakayama et al., 2002). Based on their axonal projections CINs in rodents can be anatomically classified as one of four types (Eide et al., 1999). These include: ascending commissural interneurons (aCINs), descending commissural interneurons (dCINs), bifurcating commissural interneurons (adCINs), and short-range intrasegmental commissural interneurons (sCINs).

Among the CINs, the aCINs are a unique cluster of interneurons which have long, ascending fibers providing signals to the cervical spinal cord and the brainstem and are involved in hindlimb coordination (Juvin et al., 2005). The aCINs are cholinergic interneurons (Matsuyama and Jankowska, 2004) and are activated rhythmically during fictive locomotion. This suggests that they participate in limb coordination (Zhong et al., 2006a). aCINs are also known to be composed of V0 interneurons, deletion of which leads to a hopping gait. This directly implicates them in the left-right alternations of locomotion (Lanuza et al., 2004). Although the function of aCINs have been studied widely in cats and rodents, there are few reports of the intrinsic membrane properties of these neurons and in rodents the details of their morphological and electrophysiological properties are unknown.

CINs are diverse not only in neuronal type but also in their modulatory properties. Serotonin (5-HT), acetylcholine (ACh), and N-methyl-D-aspartate (NMDA) play crucial roles in generating locomotion in rodents (Jordan et al., 2008) and have varying effects on CINs. 5-HT increases their excitability by depolarizing membrane potential and increasing input resistance (Zhong et al., 2006a). 5-HT also increases the excitability of dCINs by depolarization of membrane potential, reduction of afterhyperpolarization, and hyperpolarization of the voltage threshold for action potential generation. In addition to 5-HT, ACh induces varying

Journal of Integrative Neuroscience

effects on aCINs, including depolarization and oscillation of the membrane potential and reduction of input resistance. However, ACh has no substantial effect on aCIN voltage threshold and after-hyperpolarization (Carlin et al., 2006). Although varying effects of 5-HT and ACh on aCINs have been reported in previous studies, little is known about NMDA modulation of aCINs in rodents. In the present study, retrograde labeling and whole-cell patch clamp techniques were employed to investigate the intrinsic membrane properties of aCINs and explore the effect of NMDA on aCIN activity in rat spinal slices. Experimental results indicated that aCINs possessed unique membrane properties and that NMDA increased the excitability of aCINs.

2. Method

2.1 Animals and surgery

This study employed neonatal wild-type Wistar rats (postnatal days 1–10). Animal protocols were reviewed and approved by the East China Normal University Laboratory Animal Center and Animal Experiment Ethics Committee. The preparation of rodent spinal cord slices has previously been described (Dai and Jordan, 2011). Briefly, animals were anaesthetized with diethyl ether, decapitated, and eviscerated. The spinal cord was removed by vertebrectomy and longitudinally hemisected rostrally to the lumbar enlargement of the T12 segment.

2.2 Retrograde labeling

aCINs were labeled as previously described (Carlin et al., 2006). Briefly, a spinal cord preparation was placed in a Sylgard-lined petri dish with the hemicord. The main bath contained regular dissecting artificial cerebrospinal fluid (ACSF) bubbled with 95% O_2 and 5% CO_2. The isolated spinal cord was transected at approximately the midthoracic level and together with approximately 1.5 mm of vaseline wall was injected with 25% dextran tetramethylrhodamine (TMR, Life; D3308) in the cut end (Fig. 1A) using a manual microinjection pump (WPI, MMP, USA). Two types of aCINs were labeled in this way. One type had axons projecting to the contralateral side of the spine and the other had dendrites that crossed the midline. Bifurcating neurons, with both ascending and descending axons were also labeled. For simplicity, these three groups of neurons are collectively referred to here as aCINs.

2.3 Slice preparation

Transverse spinal cord slices were prepared for electrophysiological experiment after 2.5 to 6 hours retrograde labelling. The unseparated part of the lumbar spinal cord was blocked and mounted on a Leica vibrating microtome (VT 1000E, Germany) and filled with 4°C dissecting ACSF. Slices (250 μm) were cut and placed into recording ACSF and left to recover for one hour at room temperature.

2.4 Patch-clamp recordings

Slices were transferred into a 1 ml recording chamber mounted in the stage of an upright Olympus BX50 microscope fitted with differential interference contrast optics and epifluorescence. Recording ACSF bubbled with 95% O_2 and 5% CO_2 was supplied via gravity perfusion system (flow rate 2 ml/minute). Neurons were visualized using infrared illumination and images collected with a Hamamatsu camera (ORCA-Flash 2.8 and ARGUS image processor). aCINs were then identified with red fluorescence fil-

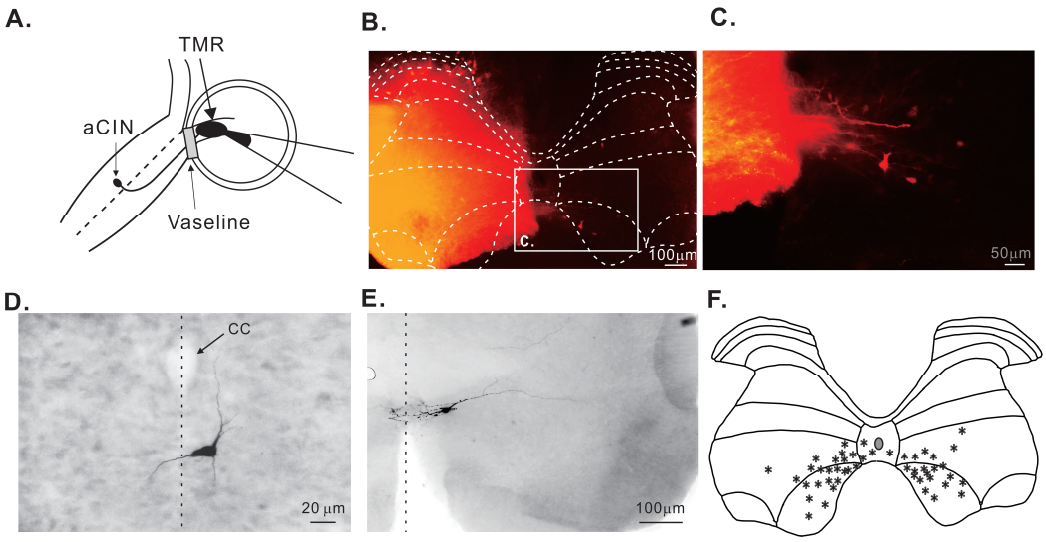

Figure 1. Retrograde labeling of aCINs. A: Labeling procedure for aCNs in spinal cord. Rostral portion of cord was hemisected with one hemicord placed in a small well filled with hydrophobic silicon oil and sealed with Vaseline. Dextran tetramethylrhodamine solution (25%) was injected into the cut end. Axons of ascending CINs crossed to the contralateral side and absorbed the dye which then labeled aCINs. B: Slice (250 μm) from the upper lumbar region showed retrograde-labeled aCINs with axons crossing in the ventral commissure. The left side was dye-injected and aCINs in the right side were labeled mainly in laminae VII and VIII. C: Enlarged box in panel B (lebeled C) shows details of retrogradely labeled aCINs with fibers. D: Lucifer yellow filled aCIN. Neuron located in lamina X with axon projecting to contralateral side. Dashed line indicates spinal cord midline. CC (central canal, indicated by arrow). E: aCIN located in lamina VIII with dendrites crossing midline. F: Laminar distribution of 48 aCINs patched for data analysis in this study (shown as asterisks).

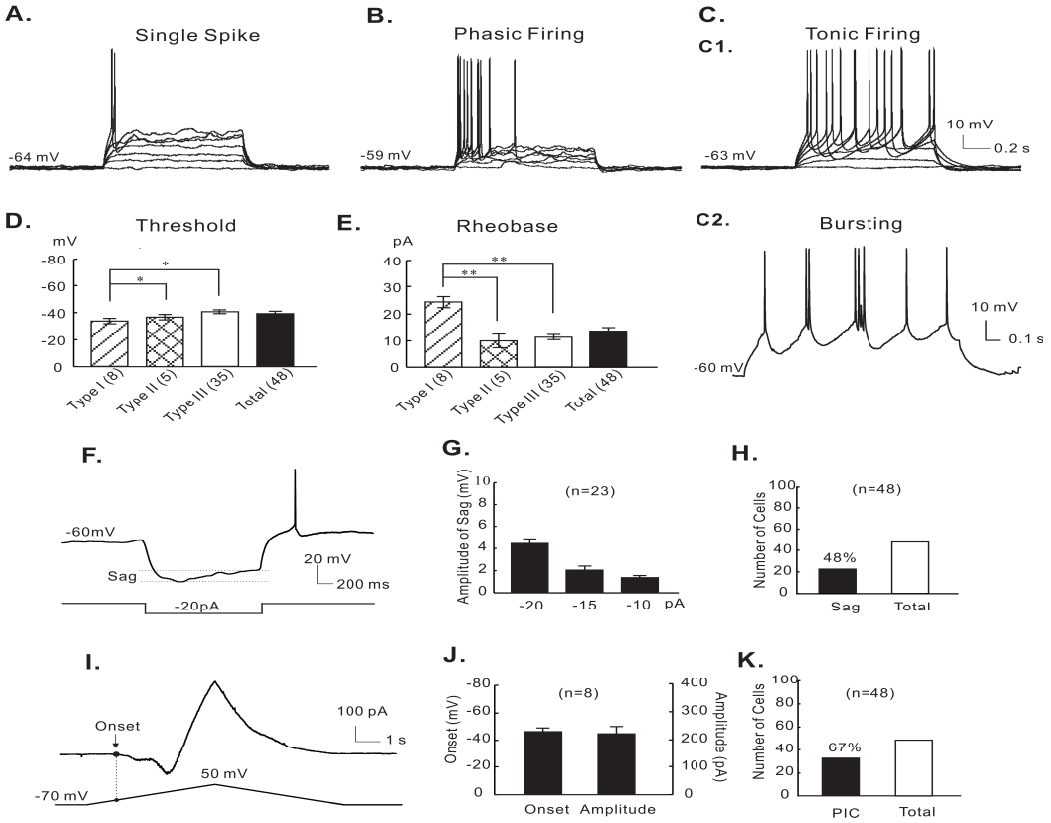

Figure 2. Electrophysiological properties of three types of aCIN. A: Step currents (pulse magnitude increased by 5 pA–one second duration–for each stimulus ranging from 0–30 pA) were injected into a type I aCIN. Single spike was elicited at the fifth magnitude (25 pA). B: The same step currents evoked a brief 500 ms firing in a type II aCIN. C. Tonic firing was evoked by same depolarizing step current (C1). Burst firing, a special tonic firing, was also observed in aCINs (C2). Statistical analysis of V_{th} (D) and rheobase (E) revealed three types of aCIN. D: The V_{th} of type I aCINs (-33.8 ± 1.4 mV, n = 8) was significantly depolarized ($*P < 0.05$) from that of type II (-37.4 ± 1.8 mV, n = 5) and type III (-40.9 ± 0.6 mV, n = 35) aCINs. No significant difference was found between type II and type III aCINs. E: Statistical analysis showed that the rheobase of type I aCINs (24.5 ± 1.7 pA, n = 8) was significantly larger ($*P < 0.05$) than that of type II aCINs (10.0 ± 2.4 pA, n = 5) and type III (11.5 ± 1.0 pA, n = 35), while no significant difference was found between type II and type III aCINs. F: A hyperpolarization activated inward current (*Ih*) was activated by injecting a step current of -20 pA and 1.5 second duration into a type III aCIN located in lamina VIII. *Ih* showed a depolarizing sag with the two dashed lines used to calculate the sag value (10.4 mV in this case). Post inhibitory rebound spike elicited after the termination of the step current is seen. G: Relation between sag and injected current was established from 23 aCINs. A sag with an amplitude of 4.5 ± 0.3 mV, 2.1 ± 0.4 mV, and 1.4 ± 0.2 mV was induced by -20 pA, -15 pA and -10 pA current pulses, respectively. H: Sag was observed in 48% of the 48 aCINs. I: A 10-second voltage ramp from -70 to 50 mV was applied to an aCIN in lamina VIII and the persistent inward current (PIC) was evoked on the rising phase of the voltage ramp with an onset of -49.3 mV and amplitude of 163.5 pA. J: Onset (at -47.5 ± 1.3 mV) and amplitude (248.9 ± 33.6 pA) of PIC were calculated from eight aCINs recorded with 10 mM TEA in ACSF. K: PIC was observed in 67% of 48 aCINs.

ter and patched under infrared illumination by glass electrodes, resistance 6–8 MΩ. Lucifer yellow (∼1%, MW: 457.2442, life: L453) was added to the intracellular solution in some experiments to study the morphology of the recorded aCINs. A MultiClamp 700B amplifier, Digidata 1550B A/D converter, Minidigi 1B, and pClamp (10.7) software (all from Molecular Devices) were used for data acquisition. Whole cell patch recordings were made in current and voltage clamp mode with bridge balance. Data were low-filtered at 3 kHz and sampled at 10 kHz.

2.5 Electrophysiological data analysis

All electrophysiological data were analyzed with Clampfit (10.7). The parameters measured and calculated in this study included the resting membrane potential (E_m), input resistance (R_{in}), voltage threshold (V_{th}), current threshold (rheobase), membrane time constant (τ_m), whole cell capacitance (C_m), slope and intercepts of frequency-current (F-I) relation, action potential (AP) height and half-width, afterhyperpolarization (AHP) magnitude, and half-decay time. Calculation of the values of these parameters has previously been described (Dai et al., 2009). To avoid slice cutting damage, neurons 50-100 μm below the slice surface were selected for patch clamp recording. Neurons were selected for analysis based on the criteria that the AP overshoot was $\geq$ 5 mV and $R_{in} \geq$ 250 MΩ. PIC was recorded by applying a series of slow voltage bi-ramps with duration of 10 s, steps of 40 mV, and holding potential of -70 mV. The leak current was subtracted

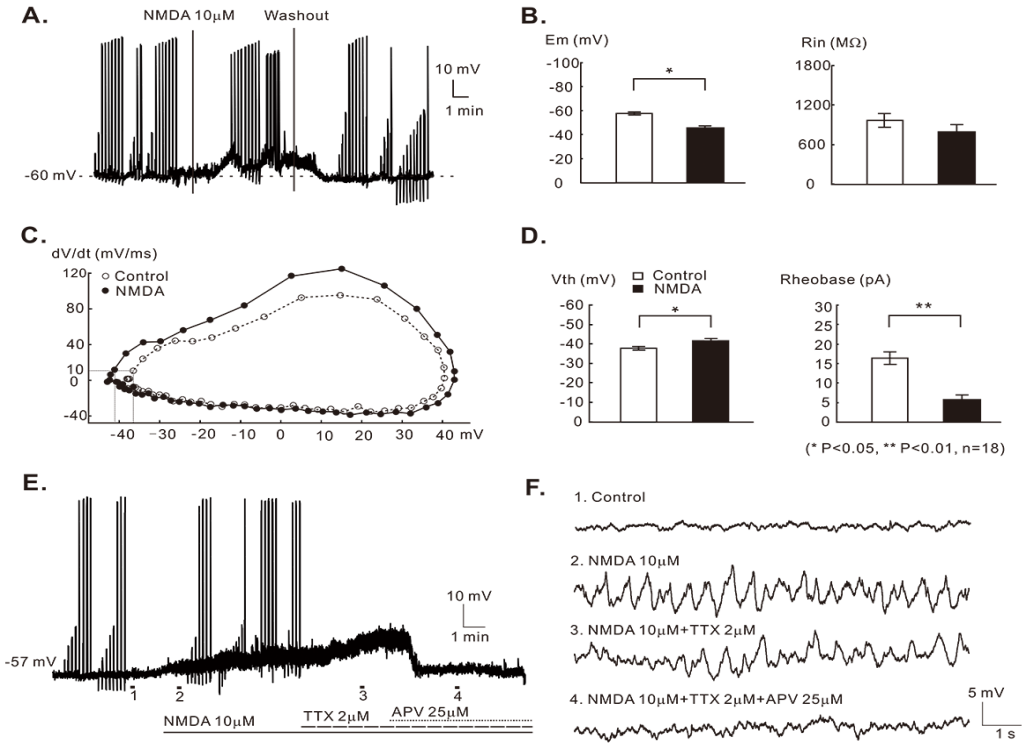

Figure 3. NMDA modulation of aCIN membrane properties. A: Bath application of 10 μM NMDA induced membrane depolarization, and effect reversed by washout. B: Analysis revealed NMDA-induced changes in resting membrane potential and R_{in} of aCINs (n = 18). NMDA significantly depolarized the resting membrane potential (control: -57.3 ± 1.2 mV, NMDA: -46.7 ± 1.6 mV, $*P < 0.05$, left panel) with a slight decrease in the input resistance (control: 987.3 ± 87.1 MΩ, NMDA: 796.8 ± 81.8 MΩ, right panel). C: V_{th} was defined as the membrane potential at which dV/dt = 10 mV/ms. NMDA hyperpolarized V_{th} by 5.2 mV in this aCIN. V_{th} was -36.3 mV in control (dash line with open circle) and -41.5 mV with NMDA (solid line with closed circle). D: Statistical summary of 18 aCINs. NMDA induced a significant hyperpolarization of V_{th} (4.8 ± 0.6 mV, control: -37.3 ± 0.6 mV, NMDA: -42.1 ± 0.7, $*P < 0.05$) and a significant reduction of rheobase (10.6 ± 1.1 pA, control: 16.6 ± 1.5 mV, NMDA: 5.9 ± 0.8, $**P < 0.01$). E: NMDA-mediated depolarization and membrane oscillation were blocked by APV. Bath application of 10 μM NMDA induced membrane oscillation, which persisted following application of 2 μM TTX. However, 25 μM APV completely eliminated the membrane depolarization and oscillations. F: Expanded views of membrane oscillation (marked 1-4 in E). (1) No substantial change in membrane potential under control conditions. (2) Application of 10 μM NMDA induced membrane potential oscillation with 3 Hz frequency and 10 mV amplitude. (3) Application of 2 μM TTX reduced the frequency of membrane oscillation to ∼2 Hz and amplitude to ∼7 mV. (4) Application of 25 μM APV completely eliminated membrane depolarization and oscillation.

from recordings before calculation of biophysical parameters. PIC evoked in the ascending phase of the voltage ramp was used for parameter calculation. The membrane voltage at which the PIC was initiated was defined as PIC onset. The difference between the onset and the lowest point of the current trough was defined as the PIC amplitude. Post hoc statistical tests followed by ANOVA were carried out to compare the intrinsic membrane properties of three different types of aCINs. Paired sample *t*-test was used to analyze the effect of NMDA on neuronal membrane properties. Student's *t*-test and ANOVA were performed with statistical significance defined as $P < 0.05$. Results are given as mean ± standard error of the mean (SEM).

2.6 Solutions and chemicals

Dissecting ACSF (mM): NaCl (25), sucrose (253), KCl (1.9), NaH_2PO_4 (1.2), $MgSO_4$ (10), $NaHCO_3$ (26), kynurenic acid (1.5), glucose (25), and $CaCl_2$ (1.0). Recording ACSF (mM): NaCl (125), KCl (2.5), $NaHCO_3$ (26), NaH_2PO_4 (1.25), glucose (25), $MgCl_2$ (1), and $CaCl_2$ (2.0). Intracellular solution for current clamp (mM): K-gluconate (135), NaCl (10), HEPES (10), $MgCl_2$ (2), Mg-ATP (5), and GTP (0.5). Solution pH was adjusted to 7.3 with HCl and osmolarity adjusted to 305 mOsm by sucrose addition.

Drugs: 10 μM APV (A5282 Sigma) a NMDA receptor antagonist and 1–2 μM Tetrodotoxin (TTX HY-12526, MCE) a transient sodium channel blocker were used to block synaptic transmission. 10 μM NMDA (M3263 Sigma) was used to activate NMDA receptors. TEA (T2265 Sigma) was used to block potassium channels. Eight neurons were recorded with 10 mM TEA added to the recording ACSF and 20 mM TEA in the pipette solution. Data from these neurons were used to calculate PIC onset and amplitude.

3. Results

3.1 Distribution and morphology of aCINs

The dye-injected side of slices were much brighter than the contralateral side where fluorescence positive neurons were rec-

Table 1. Membrane properties of three types of aCINs

	Type 1 (8)	Type 2 (5)	Type 3 (35)	Mean (48)	Significance		
					Type1 vs. 2	Type 2 vs. 3	Type 1 vs. 3
E_m, mV	-59.6 ± 3.1	-54.6 ± 1.5	-60.8 ± 0.9	-59.2 ± 0.8	NS	NS	NS
R_{in}, MΩ	973.4 ± 116.5	751.2 ± 77.2	989.7 ± 97.8	964.4 ± 49.3	NS	NS	NS
V_{th}, mV	-33.8 ± 1.4	-37.4 ± 1.8	-40.9 ± 0.6	-39.5 ± 0.6	*	NS	*
Rheobase. pA	24.5 ± 1.7	10.0 ± 2.4	11.5 ± 1.0	13.5 ± 0.77	**	NS	**
τ_m, ms	38.3 ± 5.3	43.0 ± 9.2	51.4 ± 3.4	48.7 ± 2.9	NS	NS	NS
C_m, pF	46.8 ± 5.1	61.9 ± 19.7	57.3 ± 3.2	56.0 ± 3.1	NS	NS	NS
AP height, mV	51.7 ± 5.9	53.9 ± 11.3	56.6 ± 2.5	55.6 ± 2.2	NS	NS	NS
AP half-width, ms	2.8 ± 0.4	2.9 ± 0.2	2.8 ± 0.1	2.8 ± 0.1	NS	NS	NS
AHP depth, mV	17.4 ± 1.1	14.2 ± 4.3	15.9 ± 1.5	16.1 ± 1.2	NS	NS	NS
AHP 1/2 decay, ms	149.7 ± 30.8	250.8 ± 30.5	229.9 ± 11.1	217.9 ± 10.7	NS	NS	NS
Lamina VII	3	3	10				
Lamina VIII	4	2	21				
Lamina	1	0	4				

Values in parentheses are number of aCINs. Data are represented as means ± SEM. * significant difference with $P < 0.05$, ** significant difference with $P < 0.01$, NS: no significant difference.

ognized as aCINs. Fig. 1B shows an example of aCINs labeled in a lumbar segment. The injected left side was much brighter than the right side where a cluster of aCINs and a nerve fiber bundle are labeled in laminas VIII and VII. The boxed area of Fig. 1B, enlarged in Fig. 1C, illustrates the many aCINs labeled in laminas VII and VIII.

Fig. 1F illustrates the laminar distribution of the 48 aCINs recorded in this study. These aCINs were mainly located in laminas VII and VIII (90%, 43/48), with a small portion in lamina X (10%, 5/48). Two types of aCIN were labeled. One type had axons that projected to the contralateral side of the spinal cord (Fig. 1D, example in lamina X) and the other type had dendrites that crossed to the midline (Fig. 1E, example in lamina VIII). These aCINs were identified by tetramethylrhodamine and patched with a glass electrode filled with Lucifer yellow.

3.2 Three types of aCINs firing pattern

Electrophysiological data were collected from 48 aCINs labeled by fluorescence dye. aCINs could be classified into three types based on their firing pattern in response to depolarizing current steps. A series of depolarizing step currents were injected into recorded neurons, and type I aCINs (single spike) generated only one or two action potentials during the stimulus pulse (Fig. 2A). Type II (phasic) firing of aCINs was brief with a duration < 1 s (Fig. 2B) and type III (tonic) activity evoked repetitive firing during the current injection (Fig. 2C 1). Of the 48 recorded neurons, three displayed burst patterns of firing (Fig. 2C 2) classified as type III. Similar firing patterns have been reported in a previous study of rodent spinal neurons (Dai et al., 2009). Results reported here showed the number of type I (8/48) and type II (5/48) aCINs was significantly less than the number of type III firing patterns (35/48, $P < 0.05$). Table 1 summarizes the membrane properties of the three identified types of aCINs. Generally, V_{th} of type I aCINs (-33.8 ± 1.4 mV, n = 8) was significantly higher than that of type II (-37.4 ± 1.8 mV, n = 5) and type III aCINs (-40.9 ± 0.6 mV, n = 35) ($P < 0.05$) and there was no significant difference in V_{th} between type II and type III aCINs (Fig. 2D). Similar results were also obtained for rheobase. The rheobase of type I aCINs (24.5 ± 1.7 pA, n = 8) was significantly greater than that of type II (10.0 ± 2.4 pA, n = 5) and type III aCINs (11.5 ± 1.0 pA, n = 35) ($P < 0.01$), while there was no statistical difference in rheobase between type II and III aCINs (Fig. 2E). Since V_{th} and rheobase were essential parameters used to describe neuronal excitability, these data suggested that the excitability of type I aCINs should be lower than that of the other two types.

3.3 Membrane currents mediated by multiple channels

The hyperpolarization-activated nonselective cation current (*Ih*)-mediated sag in aCINs was studied in neonatal rats. Fig. 2F shows an example of the sag triggered in a type III neuron located in lamina VIII by a 1.5 second duration -20 pA amplitude current pulse. A post-inhibitory rebound was elicited in this neuron after pulse termination. A sag in the membrane potential was observed in 23 of 48 neurons (48%) recorded in aCINs (Fig. 2H). Furthermore, the amplitude of the *Ih*-mediated sag was shown to be current-dependent (Fig. 2G). Of 23 aCINs analyzed for sag amplitude, -20 pA, -15 pA, and -10 pA current steps induced sags of 4.5 ± 0.3 mV, 2.1 ± 0.4 mV, and 1.4 ± 0.2 mV, respectively. The current pulse determined the extent of membrane hyperpolarization which in turn determined the sag amplitude. Of the 23 aCINs expressing sag, three were located in lamina X, seven in lamina VII, and thirteen in lamina VIII. No correlation was found between sag occurrence and laminar distribution.

The properties of PIC were also investigated in aCINs of neonatal rats. PIC was induced by a slow voltage ramp as shown in Fig. 2I, where a 10-second voltage was ramped from -70 to 50 mV in an aCIN located in lamina VIII. Analysis of 48 aCINs revealed PIC was expressed in 67% of neurons (32/48, Fig. 2K). PIC was activated at -47.5 ± 1.3 mV with an amplitude of 248.9 ± 33.6 pA (n = 8, Fig. 2J), similar to a previous report of spinal interneurons of neonatal mice (Dai and Jordan, 2010a,b). No correlation was found between PIC activity and laminar distribution of the aCINs.

3.4 NMDA modulation of aCINs

Previous studies have shown that endogenous glutamate released via NMDA receptors (NMDARs) regulates the frequency of step cycles and contributes to gait selection during locomotion in mammals (Kiehn et al., 2008; Talpalar and Kiehn, 2010). Recent study has also shown that NMDA alone could lead to a robust left/right alternation during fictive locomotion in isolated spinal cord (Acton and Miles, 2017; Talpalar et al., 2013). Based on these results, the modulatory effect of NMDA on aCINs was studied, as was the potential cellular role of the NMDA pathway in regulating left-right limb coordination during locomotion.

3.4.1 NMDA regulation of aCIN excitability

The effect of NMDA on the membrane properties of aCINs was also investigated. 10 μM NMDA depolarized the membrane potential and increased excitability of aCINs. An example is given in Fig. 3A, the membrane potential of the aCIN was clearly depolarized by 10 μM NMDA and the effect disappeared with washout. NMDA-induced depolarization with tonic firing was observed in 44% of aCINs (8/18). Analysis of 18 aCINs (Table 2) showed that the cell membrane was significantly depolarized (10.6 ± 0.6 mV, $P < 0.05$, Fig. 3B left panel) from -57.3 ± 1.2 mV to -46.7 ± 1.6 mV. NMDA also induced a nonsignificant reduction of R_{in} (190.5 ± 80.0 MΩ, control: 987.3 ± 87.1 MΩ, NMDA: 796.8 ± 81.8 MΩ, Fig. 3B, right panel).

In addition to alteration of resting membrane potential and input resistance, NMDA also induced changes in V_{th} and rheobase. Data showed that applications of NMDA lowered V_{th} and decreased rheobase. A typical example is shown in Fig. 3C, where V_{th} was lowered by 5.2 mV from -36.3 mV to -41.5 mV with 10 μM NMDA. NMDA significantly hyperpolarized the voltage threshold by 4.8 ± 0.6 mV (Table 2, Fig. 3D left panel, n = 18, $P < 0.05$) and reduced the rheobase by 10.6 ± 1.1 pA (Table 2, Fig. 3D right panel, n = 18, $P < 0.01$). This suggests that NMDA could increase aCIN excitability.

3.4.2 NMDA induced membrane oscillation

It was further demonstrated that NMDA could induce membrane oscillation in aCINs. An example is given in Fig. 3E where bath application of 10 μM NMDA depolarized the membrane and evoked oscillation of the membrane potential (Fig. 3F). The oscillation persisted with a small reduction of amplitude (1–2 mV) and frequency (~1 Hz) after application of 2 μM TTX. This oscillation could be completely eliminated by APV (25 μM), suggesting that NMDA acted directly on postsynaptic receptors of aCINs and regulated intrinsic membrane properties. 61% of aCINs (11 /18) exhibited membrane oscillation after bath application of 10 μM NMDA. The peak-to-peak amplitude of oscillation was 6.2 ± 0.6 mV and the frequency was 3.1 ± 0.3 Hz (n = 11).

3.4.3 F-I relationship regulated by NMDA

The effect of NMDA on the F-I relationship of aCINs was also specifically explored. A typical experiment is shown in Fig. 4A, where repetitive firing was evoked by a step current (20 pA) injected into an aCIN (Fig. 4A1). Bath application of 10 μM NMDA increased the number of action potentials and induced spontaneous

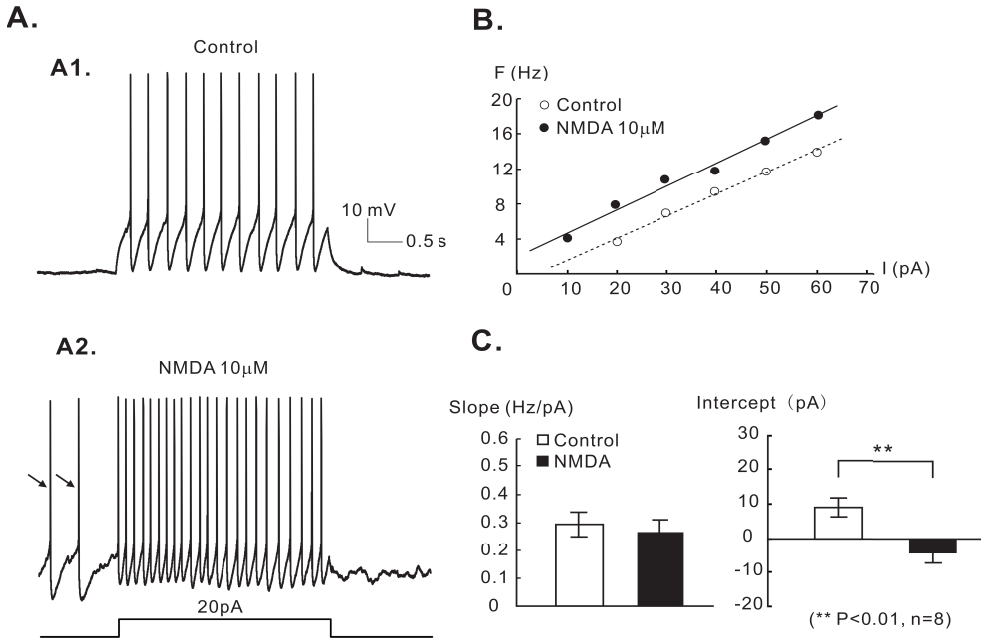

Figure 4. NMDA modulation of F-I relationship. A: Repetitive firing evoked by 20 pA step current injection (3 s duration) into an aCINs (A1). Bath application of 10 μM NMDA increased spike number from 11 to 23 (arrows indicate spontaneous firing) (A2). B: F-I relationships established under control conditions (K = 0.25 Hz/pA, I = 3.9 pA, dashed line, open circles) and NMDA (K = 0.27 Hz/pA, I = -7.3 pA solid line, closed circles). NMDA induced an increase in slope (△K = 0.02 Hz/pA) and left-shifed the F-I relationship (△I = -11.2 pA). C: Statistical analysis of slopes and intercepts of F-I relationship calculated from eight aCINs. NMDA did not have a significant effect on F-I slope (△K = -0.03 ± 0.04 Hz/pA, Control: 0.3 ± 0.04 Hz/pA, NMDA: 0.27 ± 0.04 Hz/pA, left panel) but did significantly left-shift F-I curves (△I = -13.9 ± 2.0 pA, Control: 9.2 ± 2.4 pA, NMDA: -4.7 ± 2.7 pA, $**P < 0.01$, right panel).

firing (marked with arrows, Fig. 4A2). The F-I relationship of this neuron was established through injection of a series of incremental current pulses (Fig. 4B). NMDA shifted the F-I relationship to the left (ΔI = -11.2 pA; control: I-intercept = 3.9 pA, NMDA: I-intercept = -7.3 pA) with little change in the slope in this neuron (ΔK = 0.015 Hz/pA; control: K = 0.25 Hz/pA, NMDA: K = 0.27 Hz/pA). Statistical results showed that NMDA significantly shifted the F-I relationships to the left (Control: I-intercept = 9.2 ± 2.4 pA, NMDA: I-intercept = -4.7 ± 2.7 pA, ΔI = -13.9 ± 2.0 pA, $P < 0.01$, n = 8) without substantial alteration of the slope (Control: K = 0.3 ± 0.04 Hz/pA, NMDA: K = 0.27 ± 0.04 Hz/pA, ΔK = -0.03 ± 0.04 Hz/pA, n = 8, Fig. 4C). These data suggest that NMDA could increase aCIN excitability and thus firing rate by shifting the F-I relationship to the left.

3.4.4 NMDA modulation of ionic currents in aCIN

NMDA modulation of *Ih* and PIC was investigated in this study. Fig. 5A illustrates an example that shows a NMDA-induced reduction of an *Ih*-mediated sag. Hyperpolarizing step currents were injected into an aCIN and a depolarizing sag was triggered in the initial phase of the hyperpolarized membrane potential of the last two current pulses (Fig. 5A, up trace). Bath application of 10 μM NMDA almost completely removed sags in this neuron (Fig. 5A, middle trace). The NMDA-induced reduction of sag was seen in all six aCINs examined and the reduction was current pulse dependent. Fig. 5B shows that NMDA reduced the sag amplitude by 61% at -20 pA (control: 4.1 ± 0.8 mV, NMDA: 1.6 ± 0.6 mV, $P < 0.05$, n = 6) and 82% at -15 pA (control: 1.7 ± 0.4 mV, NMDA: 0.3 ± 0.1 mV, $p < 0.01$, n = 6). These data indicated that *Ih* was expressed in aCINs and that NMDA significantly reduced *Ih*.

The effect of NMDA on PIC was also investigated. Fig. 5C illustrates an example of PIC recorded in an aCIN. The PIC was evoked by a slow bi-voltage ramp and in this aCIN activated at -46.9 mV with an amplitude of 331.0 pA. Bath application of 10 μM NMDA hyperpolarized the onset to -54.5 mV and increased the amplitude to 483.7 pA. An NMDA-enhanced PIC was observed in all five aCINs recorded. Statistical analysis is summarized in Fig. 5D. NMDA significantly hyperpolarized onset of PIC by 11.1 ± 2.9 mV (control: -46.5 ± 2.0 mV, NMDA: -57.6 ± 2.6 mV, $P < 0.05$, n = 5) and increased the PIC amplitude by 136.6 ± 32.6 pA (control: 219.8 ± 33.9 pA, NMDA: 356.4 ± 61.6 pA, $P < 0.05$, n = 5). It was demonstrated for the first time in this study that NMDA enhanced PIC in aCINs.

4. Discussion

Using retrograde labelling, the intrinsic membrane properties of aCINs in neonatal rat spinal cord were studied and the modulation of aCINs by NMDA was specifically investigated. For the first time the expression of *Ih* and PIC in aCINs were reported and the multiple effects of NMDA on Ih and PIC demonstrated. Data showed that NMDA generally increased the neuronal excitability of aCINs through depolarization of the membrane potential, hyperpolarization of the voltage threshold, reduction of rheobase, and enhancement of PIC. NMDA also reduced the input resistance and *Ih*, leading to a reduction of aCIN excitability.

4.1 Membrane properties of aCINs

CINs are crucial components of CPGs responsible for left-right coordination during locomotion (Jankowska et al., 2005; Kiehn, 2005). Using a calcium imaging technique, Nakayama et al. (2004) showed that CINs exhibited rhythmicity during drug-induced activity in the fetal rat. Subsequently, it was found that aCINs exhibited periodic firing during fictive locomotor activity induced by NMDA and 5-HT (Zhong et al., 2006a). These studies explored the functional role and modulatory properties of CINs in rodents. Alternatively, this study specifically focused on aCINs and the modulation of their membrane properties by NMDA.

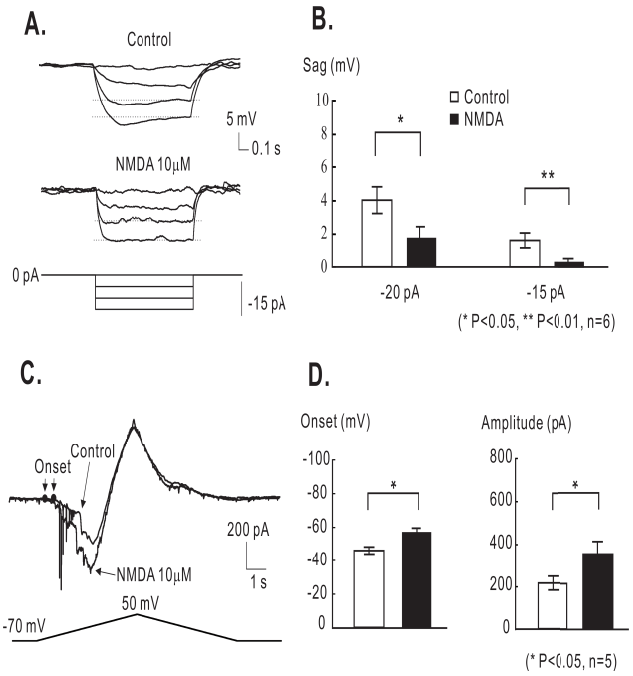

Figure 5. NMDA modulation of depolarizing sag and PIC. A: Depolarizing sags were elicited by a series of hyperpolarizing current pulses (-5 pA step, 1 s duration, bottom trace). For the control condition, two remarkable sags were elicited at -20 and -15 pA, with amplitude 2.3 mV and 1.4 mV, respectively (dashed line). Bath application of 10 μM NMDA completely removed these sags in this aCIN. B: Analysis (n = 6) showed NMDA significantly reduced the amplitude of depolarizing sag. Under control conditions, sags amplitudes were 4.1 ± 0.8 mV and 1.7 ± 0.4 mV in response to -20 pA and -15 pA current pulses, respectively. NMDA reduced the sag to 1.6 ± 0.6 mV and 0.3 ± 0.1 mV in response to -20 pA and -15 pA current pulses, respectively (*$P < 0.05$ at -20 pA and **$P < 0.01$ at -15 pA). C: NMDA enhanced the PIC in aCINs. PICs were evoked by a 10 s bi-voltage ramp from -70 to 50 mV (bottom trace). Bath application of 10 μM NMDA hyperpolarized the onset potential of PIC by 7.5 mV (control: -46.9 mV; NMDA: -54.5 mV) and increased the amplitude by 152.7 pA (control: 331.0 pA; NMDA: 483.7 pA) in this aCIN. D: Statistical analysis of five aCINs showed NMDA significantly hyperpolarized PIC onset by 11.1 ± 2.9 mV (*$P < 0.05$, control: -46.5 ± 2.0 mV, NMDA: -57.6 ± 2.6 mV) and increased PIC amplitude by 136.6 ± 32.6 mV (*$P < 0.05$, control: 219.8 ± 33.9 pA, NMDA: 356.4 ± 61.6 pA).

Similarly, as reported by previous studies of CINs (Carlin et al., 2006; Zhong et al., 2006a,b) and locomotion-related spinal interneurons (Dai et al., 2009), aCINs were found to exhibit three types of firing pattern which were determined intrinsically by passive and active membrane properties of the neurons. The different excitabilities of aCINs suggested that they might play different functional roles in locomotion. The major active properties (V_{th}, AP height, and AHP depth, see Table 1) of the three types of aCIN are generally similar to those of the corresponding types of spinal interneuron (difference < 20%). This suggested that the aCINs examined in this study should belong to the interneuron clusters that participate in the generation of locomotion.

Table 2. Membrane properties of aCINs modulated by NMDA

	Control (n = 18)	NMDA (n = 18)	Change
E_m, mV	-57.3 ± 1.2	-46.7 ± 1.6	10.6 ± 0.6*
R_{in} , MΩ	987.3 ± 87.1	796.8 ± 81.8	-190.5 ± 80.0
V_{th}, mV	-37.3 ± 0.6	-42.1 ± 0.7	-4.8 ± 0.6*
rheobase, pA	16.6 ± 1.5	5.9 ± 0.8	-10.6 ± 1.1**
τ_m, ms	48.2 ± 2.9	46.5 ± 3.9	-1.7 ± 4.5
C_m, pF	56.4 ± 3.6	60.6 ± 5.7	4.2 ± 5.5
AP height, mV	57.7 ± 2.1	52.0 ± 1.6	-5.7 ± 1.0
AP half-width, ms	2.5 ± 0.04	2.8 ± 0.1	0.3 ± 0.05
AHP depth, mV	20.4 ± 0.8	19.7 ± 0.9	-0.7 ± 0.4
AHP 1/2 decay, ms	263.5 ± 15.3	224.2 ± 18.8	-39.3 ± 23.1

Values in parentheses are number of aCI

Ns. Data are represented as means ± SEM.* significant difference with $P < 0.05$, ** significant difference with $P < 0.01$.

As for postnatal development in neurons, change in the excitability of CINs with development has been shown in neonatal mice (Abbinanti et al., 2012). However, this change was not observed in the present study. Among the 48 neurons recorded in this study, 19 were collected from rats of age 1–5 days and 29 from age 6–10 days. The rats were divided into two groups (Group 1: P1–P5; Group 2: P6–P10) and the intrinsic membrane properties of aCINs under NMDA modulation were compared. Analysis showed that significant differences occurred only for input resistance and that NMDA did not induce any substantial difference between these two groups (Table 3).

4.2 Multiple effects of NMDA on excitability of aCINs

NMDA significantly depolarized the resting membrane potential, hyperpolarized voltage threshold, and reduced rheobase (Fig. 3, Table 2). These changes increased aCIN excitability. Alternatively, however, NMDA also substantially reduced input resistance, resulting in decreased aCIN excitability (Fig. 3B). Similar results were reported in previous studies when aCINs were modulated with either 5-HT (Zhong et al., 2006a) or ACh (Carlin et al., 2006). 5-HT induced depolarization of the resting membrane potential, broadened the action potential, and reduced the AHP amplitude of aCINs, while application of ACh depolarized the resting membrane potential and reduced input resistance. The complex of changes induced by NMDA, 5-HT, and ACh generally increased the excitability of aCINs. Another important characteristic of aCINs is NMDA-induced membrane oscillation. This is an essential property for facilitation of locomotion and has been demonstrated in rodents (Hochman et al., 1994; Schmidt et al., 1998) and other species (Wang et al., 2014). Interestingly, similar membrane oscillations have been reported for aCINs modulated by 5-HT and ACh in rodents (Carlin et al., 2006). These results suggest that aCINs could form unique clusters of spinal interneurons modulated by major excitatory neurotransmitters, particularly NMDA, involved in the facilitation of left-right limb alternation during locomotion.

4.3 NMDA modulation of Ih and PIC

Both *Ih* and PIC were detected in aCINs in this study. *Ih* is one of the channel mechanisms underlying rhythmic pattern generation such as locomotion (Kiehn et al., 2000) and respiration (Thoby-Brisson et al., 2000). This current had been reported in dCINs and aCINs by a previous study (Butt et al., 2002). However, NMDA modulation of *Ih* in aCINs remained unclear. In this study an *Ih*-mediated sag in aCINs was revealed and it was further shown that NMDA reduced this sag. Different from the effect of 5-HT, which diversely affects *Ih* in CINs (Zhong et al., 2006a,b) and locomotion-activated spinal interneurons (Dai and Jordan, 2010b), NMDA universally reduced the *Ih*-mediated sag in aCINs and when accompanied by reduction of input resistance this could decrease the excitability of aCINs.

Contrary to the effect of NMDA on Ih, NMDA enhanced PIC in all aCINs studied. This appeared as an increase in the amplitude and hyperpolarization of PIC onset, which led to increased aCIN excitability. This suggests that a NMDA-enhanced PIC could potentially provide an ionic basis by which aCINs could contribute to coordination of locomotion. The opposite effects of NMDA on *Ih* and PIC were first reported for aCINs by this study, and their functional impact on locomotion remains unknown. However, as NMDA is required to generate locomotion (Cazalets et al., 1996) and *Ih* and PIC exhibit essential roles in regulating neuronal excitability (Dai and Jordan, 2010a,b), the multiple effects of NMDA on *Ih* and PIC in aCINs suggest that multi-regulated neuronal excitability may be balanced or maximized by the spinal motor control system for generation of locomotion (Dai et al., 2018) and that NMDA may play a unique role in modulation of aCIN activity during locomotion.

4.4 Membrane oscillations induced by NMDA

Membrane oscillation is one important characteristic of spinal neurons related to the generation of locomotion. The $V0_V$ interneurons, a cluster of genetically identified CINs, displayed membrane oscillations with coordination of fictive locomotion (Rebecka and Abdeljabbar, 2016). In rat slice preparation the membrane oscillations of aCINs could be induced by administration of 5-HT or ACh, and these oscillations persisted in the presence of TTX, suggesting that the oscillations should be induced by intrinsic mechanisms of the aCINs (Carlin et al., 2006). In the current study NMDA induced membrane oscillation was demonstrated in aCINs and this activity was TTX resistant. This further suggests that NMDA could directly act on postsynaptic receptors of aCINs and regulate an intrinsic membrane property. Thus, NMDA-induced membrane oscillation enabled aCINs to participate in coordination of locomotion.

Table 3. Properties of aCINs from different postnatal age groups

	Group 1 P1–5 (n = 19)	Group 2 P6–10 (n = 29)	Changed by NMDA	
			P1–5 (n = 7)	P6–10 (n = 11)
E_m, mV	-62.8 ± 1.5	-58.3 ± 0.7	11.5 ± 2.7	9.8 ± 0.7
R_{in}, MΩ	920.7 ± 181.0	1032 ± 94.9*	-199.5 ± 182.6	-187.5 ± 60.2
V_{th} , mV	-38.6 ± 1.3	-39.4 ± 0.9	-4.5 ± 1.6	-4.9 ± 0.4
Rheobase. pA	14.3 ± 1.9	12.2 ± 0.9	-9.2 ± 0.7	-10.6 ± 1.4
τ_m, ms	47.3 ± 3.7	49.4 ± 4.3	-1.3 ± 2.1	-1.9 ± 1.7
C_m, pF	46.8 ± 5.1	59.3 ± 12.7	4.1 ± 4.3	4.8 ± 5.1
AP height, mV	53.4 ± 3.1	57.2 ± 2.7	-6.6 ± 3.1	-4.7 ± 1.1
AP half-width, ms	3.1 ± 0.2	2.7 ± 0.1	0.2 ± 0.03	0.5 ± 0.04
AHP depth, mV	14.1 ± 2.1	16.3 ± 1.0	-0.9 ± 0.7	-0.7 ± 0.6
AHP 1/2 decay, ms	199.3 ± 16.6	219.3 ± 10.1	-35.7 ± 31.9	-41.3 ± 30.1

Data are represented as mean ± SEM. *$P < 0.05$ significantly different from group 1 (P1–5).

5. Conclusions

It was shown that an H-current and PIC were expressed in aCINs. NMDA increased the excitability of aCINs through modulation of their intrinsic ionic properties. NMDA modulation of aCINs allowed this interneuron cluster to potentially perform unique functions during walking.

Acknowledgment

This study was supported by National Natural Science Foundation of China (No. 31571222) and Contingent Construction Funds of East China Normal University (No. 11000-5154C1-15068) to YD.

Authors' Contributions

Yi Cheng and Yue Dai designed the study. YC performed the experiments and wrote the manuscript. KC and RG analyzed the data. YD modified the manuscript.

Conflict of interest

The authors declare no conflicts of interest.

Submitted: January 24, 2019

Accepted: May 12, 2019

Published: June 30, 2019

References

Abbinanti, M. D., Zhong, G. and Harris-Warrick, R. M. (2012). Postnatal emergence of serotonin-induced plateau potentials in commissural interneurons of the mouse spinal cord. *Journal of Neurophysiology* **108**, 2191-2202.

Acton, D. and Miles, G. B. (2017) Differential regulation of NMDA receptors by d-serine and glycine in mammalian spinal locomotor networks. *Journal of Neurophysiology* **117**, 1877-1893.

Butt, S. J., Harris-Warrick, R. M. and Kiehn, O. (2002) Firing properties of identified interneuron populations in the mammalian hindlimb central pattern generator. *Journal of Neuroscience* **22**, 9961-9971.

Carlin, K. P., Dai, Y. and Jordan, L. M. (2006) Cholinergic and serotonergic excitation of ascending commissural neurons in the thoraco-lumbar spinal cord of the neonatal mouse. *Journal of Neurophysiology* **95**, 1278-1284.

Cazalets, J. R., Borde, M. and Clarac, F. (1996) The synaptic drive from the spinal locomotor network to motoneurons in the newborn rat. *Journal of Neuroscience* **16**, 298-306.

Dai, Y., Carlin, K. P., Li, Z., McMahon, D. G., Brownstone, R. M. and Jordan, L. M. (2009) Electrophysiological and pharmacological properties of locomotor activity-related neurons in cfos-EGFP mice. *Journal of Neurophysiology* **102**, 3365-3383.

Dai, Y., Cheng, Y., Fedirchuk, B., Jordan, L. M. and Chu, J. (2018) Motoneuron output regulated by ionic channels: a modeling study of motoneuron frequency-current relationships during fictive locomotion. *Journal of Neurophysiology* **120**, 1840-1858.

Dai, Y. and Jordan, L. M. (2010a) Multiple patterns and components of persistent inward current with serotonergic modulation in locomotor activity-related neurons in Cfos-EGFP mice. *Journal of Neurophysiolog* **103**, 1712-1727.

Dai, Y. and Jordan, L. M. (2010b) Multiple effects of serotonin and acetylcholine on hyperpolarization-activated inward current in locomotor activity-related neurons in Cfos-EGFP mice. *Journal of Neurophysiolog* **104**, 366-381.

Dai, Y. and Jordan, L. M.(2011) Tetrodotoxin-, dihydropyridine-, and riluzole-resistant persistent inward current: novel sodium channels in rodent spinal neurons. *Journal of Neurophysiology* **106**, 1322-1340.

Eide, A. L., Glover, J., Kjaerulff, O. and Kiehn, O. (1999) Characterization of commissural interneurons in the lumbar region of the neonatal rat spinal cord. *Journal of Comparative Neurology* **403**, 332-345.

Hochman, S., Jordan, L. M. and Schmidt, B. J. (1994) TTX-resistant NMDA receptor-mediated voltage oscillations in mammalian lumbar motoneurons. *Journal of Neurophysiology* **72**, 2559-2562.

Jankowska, E. (2008) Spinal interneuronal networks in the cat: elementary components. *Brain Research Reviews* **57**, 46-55.

Jankowska, E., Krutki, P. and Matsuyama, K. (2005) Relative contribution of Ia inhibitory interneurones to inhibition of feline contralateral motoneurones evoked via commissural interneurones. *Journal of Physiology (London)* **568**, 617-628.

Jordan, L. M., Liu, J., Hedlund, P. B., Akay, T. and Pearson, K. G. (2008) Descending command systems for the initiation of locomotion in mammals. *Brain Research Reviews* **57**, 183-191.

Juvin, L., Simmers, J. and Morin, D. (2005) Propriospinal circuitry underlying interlimb coordination in mammalian quadrupedal locomotion. *Journal of Neuroscience* **25**, 6025-6035.

Kiehn, O. (2005) Locomotor circuits in the mammalian spinal cord. *Annual Review of Neuroscience* **29**, 279-306.

Kiehn, O., Kjaerulff, O., Tresch, M. C. and Harris-Warrick, R. M. (2000) Contributions of intrinsic motor neuron properties to the production of rhythmic motor output in the mammalian spinal cord. *Brain Research Bulletin* **53**, 649-659.

Kiehn, O., Quinlan, K. A., Restrepo, C. E., Lundfald, L., Borgius, L., Talpalar, A. E., et al. (2008) Excitatory components of the mammalian locomotor CPG. *Brain Research Reviews* **57**, 56-63.

Lanuza, G. M., Gosgnach, S., Pierani, A., Jessell, T. M. and Goulding, M. (2004) Genetic identification of spinal interneurons that coordinate left-right locomotor activity necessary for walking movements. *Neuron* **42**, 375-386.

Matsuyama, K. and Jankowska, E. (2004) Coupling between feline cerebellum (fastigial neurons) and motoneurons innervating hindlimb muscles. *Journal of Neurophysiology* **91**, 1183-1192.

Nakayama, K., Nishimaru, H. and Kudo, N. (2002) Basis of changes in left-right coordination of rhythmic motor activity during development in the rat spinal cord. *Journal of Neuroscience* **22**, 10388-10398.

Nakayama, K., Nishimaru, H. and Kudo, N. (2004) Rhythmic motor activity in thin transverse slice preparations of the fetal rat spinal cord. *Journal of Neurophysiology* **92**, 648-652.

Rebecka, B. E. and Abdeljabbar, E. M. (2016) Functional diversity of excitatory commissural interneurons in adult zebrafish. *ELife* **5**, 1-15.

Schmidt, B. J., Hochman, S. and MacLean, J. N. (1998) NMDA receptor-mediated oscillatory properties: potential role in rhythm generation in the mammalian spinal cord. *Annals of the New York Academy of Sciences* **860**, 189-202.

Talpalar, A. E., Bouvier, J., Borgius, L., Fortin, G., Pierani, A. and Kiehn, O. (2013) Dual-mode operation of neuronal networks involved in left–right alternation. *Nature* **500**, 85-88.

Talpalar, A. E. and Kiehn, O. (2010) Glutamatergic mechanisms for speed control and network operation in the rodent locomotor CPG. *Frontiers in Neural Circuits* **4**, 1-14.

Thoby-Brisson, M., Telgkamp, P. and Ramirez, J. (2000) The role of the hyperpolarization-activated current in modulating rhythmic activity in the isolated respiratory network of mice. *Journal of Neuroscience* **20**, 2994-3005.

Wang, D., Grillner, S. and Wallén, P. (2014) Endogenous release of 5-HT modulates the plateau phase of NMDA-induced membrane potential oscillations in lamprey spinal neurons. *Journal of Neurophysiology* **112**, 30-38.

Zhong, G., Diaz-Rios, M. and Harris-Warrick, R. M. (2006a) Serotonin modulates the properties of ascending commissural interneurons in the neonatal mouse spinal cord. *Journal of Neurophysiology* **95**, 1545-1555.

Zhong, G., Diaz-Rios, M. and Harris-Warrick, R. M. (2006b) Intrinsic and functional differences among commissural interneurons during fictive locomotion and serotonergic modulation in the neonatal mouse. *Journal of Neuroscience* **26**, 6509-6517.